

Nanostructured Boron Doped Diamond Electrodes with Increased Reactivity for Solar-Driven CO₂ Reduction in Room Temperature Ionic Liquids

Peter Knittel,^{*,[a]} Franziska Buchner,^[b] Emina Hadzifejzovic,^[c] Christian Giese,^[a] Patricia Quellmalz,^[a] Robert Seidel,^[b, d] Tristan Petit,^[b] Boyan Iliev,^[e] Thomas J. S. Schubert,^[e] Christoph E. Nebel,^[a] and John S. Foord^[c]

Conductive, boron doped diamond (BDD) is an extraordinary material with many applications in electrochemistry due to its wide potential window, outstanding robustness, low capacitance and resistance to fouling. However, in photoelectrochemistry, BDD usually requires UV light for excitation, which impedes e.g., usage in CO₂ to fuel reduction. In this work, a heavily boron doped, nanostructured diamond electrode with enhanced light absorption has been developed. It is manufactured from BDD by reactive ion etching and presents a coral-like structure with pore diameters in the nanometer range, ensuring a huge surface area. The strong light absorbance of this material is clearly visible from its black

color. Consequently, the material is called *Diamond Black* (DB). Electrochemical and X-ray photoelectron spectroscopy measurements performed at near-ambient pressure conditions of water vapor demonstrate increased surface reactivity for the hydrogen-terminated DB compared to oxidized surfaces. Depending on the surface termination, the wettability and hence the electrochemically accessible area can be changed. Photoelectrochemical conversion of CO₂ was demonstrated using a Cu₂O-modified electrode in ionic liquids under solar illumination. High formic acid production rates at low catalyst deposition times can be obtained paired with an increased catalyst stability on the DB surface.

1. Introduction

The European parliament declared in November 2019 a climate emergency for Europe further stressing the drastic impact of greenhouse gas emissions to the environment worldwide.^[1] By far

the most important green-house gas is CO₂, which is rapidly increasing in concentration in the Earth's atmosphere since the Industrial Revolution, leading to global warming and hence, climate change.^[2,3] Being aware of this detrimental effect, researchers worldwide are working on effective means to reduce CO₂ to more valuable chemicals, thereby decreasing the overall amount in the atmosphere or in exhaust gases. Closing the CO₂ cycle is crucial, especially for industry relying on chemical fuel combustion, e.g., aviation, where alternative technologies are often missing and/or can only be implemented in a lengthy process.^[4]

Thus, especially the production of alternative fuels, i.e., carbon-neutral fuels, has gained significant interest in the scientific community.^[5–7] Among all technologies developed in recent years, electrochemical and photoelectrochemical reductions using sunlight seem to be the most promising, as they are able to form liquid hydrocarbon compounds, e.g., formic acid, methane, ethylene,^[8–10] that may be directly used as alternative fuel avoiding further processing steps. However, a major issue for this reduction process is the long-term efficiency, often reduced by material/catalyst degradation or abrasion, fouling, as well as electrode surface changes.^[11,12] In addition, to provide a benign catalyst available at large-scale, the photoelectrode material needs to be based on non-toxic and abundant elements.

Conductive, boron doped diamond (BDD) has been used in electrochemistry for several decades due to its intriguing properties.^[13] BDD is the mechanically most robust electrode material available to electrochemists, nowadays commonly obtained from chemical vapor deposition (CVD) or hot filament synthesis, and technologically mastered in a way that some researchers call it a designer electrode material.^[14] Additionally,


[a] Dr. P. Knittel, Dr. C. Giese, P. Quellmalz, Prof. C. E. Nebel
Fraunhofer IAF
Fraunhofer Institute for Applied Solid State Physics
Tullastraße 72
79108 Freiburg (Germany)
E-mail: peter.knittel@iaf.fraunhofer.de


[b] Dr. F. Buchner, Dr. R. Seidel, Dr. T. Petit
Helmholtz-Zentrum Berlin für Materialien und Energie GmbH
Albert-Einstein-Str. 15
12489 Berlin (Germany)

[c] Dr. E. Hadzifejzovic, Prof. J. S. Foord
Chemistry Research Laboratory
Department of Chemistry
University of Oxford
Mansfield Rd
Oxford
OX1 3TA (United Kingdom)

[d] Dr. R. Seidel
Humboldt-Universität zu Berlin
Department of Chemistry
Brook-Taylor-Str. 2
12489 Berlin (Germany)

[e] Dr. B. Iliev, Dr. T. J. S. Schubert
IOLITEC Ionic liquids Technologies GmbH
Salzstrasse 184
74076 Heilbronn (Germany)

 Supporting information for this article is available on the WWW under <https://doi.org/10.1002/cctc.202000938>

 © 2020 The Authors. Published by Wiley-VCH GmbH. This is an open access article under the terms of the Creative Commons Attribution License, which permits use, distribution and reproduction in any medium, provided the original work is properly cited.

when the diamond surface is hydrogen terminated, the diamond conduction band edge lies above the vacuum level, resulting in a so-called negative electron affinity (NEA). Thus, under illumination with UV light at a wavelength below 225 nm (5.5 eV, i.e., band gap of diamond) diamond can act as a solid-state electron emitter, not only under vacuum conditions, but also in solutions forming solvated electrons.^[15] Solvated electrons can be termed as a green, universal reducing agent with very high reducing power. However, H-terminated diamond surfaces are not stable in solution,^[16] and the high-energy radiation required for this process renders it energetically inefficient and impedes usage of light from the solar spectrum. In order to realize a diamond-based photocathode which operates in the visible spectrum, one possible way is the introduction of defect based transitions in the material by nanostructuring and boron doping.^[17]

Regarding exclusively the electrochemical reduction of CO₂, one of the outstanding properties of BDD – its chemical inertness – becomes a major problem causing low catalytic activity. Therefore, surface modifications with catalytically active nanoparticles, often achieved by simple electrodeposition, have been carried out extensively, e.g., Ag,^[18] Cu,^[19] Ce₂O₃,^[20] Cu₂O,^[21] CuO.^[22] Such modified electrodes, however, often struggle from poor adhesion of the catalytic particles, which impedes long-term operation. Although it requires more complex chemical modification routes, covalent attachment of catalyst molecules is a way to circumvent this issue.^[23]

Here, we present a heavily boron doped, nanostructured diamond electrode with enhanced visible light absorption possessing a huge surface area, which is manufactured from boron doped polycrystalline diamond by reactive ion etching (RIE) using a dewetted metal mask. Even though RIE with oxygen is a rather harsh procedure, according to Raman spectroscopy and X-ray photoelectron spectroscopy (XPS) measurements, the BDD retains its initial properties. In contrast to literature, characterization by scanning electron microscopy (SEM) reveals a coral-like structure with pore diameters in the nanometer range instead of nanowires.^[24] The strong light absorbance of the material is clearly visible from its dark black color. Consequently, the material is named *Diamond Black* (DB).

From electrochemical characterizations, an 80-fold increase in surface area, compared to the untreated film, is obtained as determined by cyclic voltammetry (CV). Experiments with redox mediators show a reversible behavior. Interestingly, the electrochemical response is contact-angle dependent, i.e., surface wettability and termination plays an important role. In addition, electrochemical and near-ambient pressure (NAP) XPS characterization demonstrate an increased surface reactivity for the H-terminated DB.

To demonstrate its practical application, the material was used in the photoelectrochemical conversion of CO₂ to liquid fuels under solar illumination. Here, room temperature ionic liquids (RTIL), termed as green solvents, are used to drastically increase the CO₂ concentration in solution,^[25] and hence the product yield compared to aqueous electrolytes. Additionally, by using a Cu₂O electrocatalyst on the diamond,^[21,26] high formic acid production rates were obtained paired with an

increased catalyst stability on the DB surface. Again, the surface termination provides an additional parameter for influencing the electrochemical modification of the diamond electrode, as the Cu₂O deposition behaves strongly different on H- and O-terminated DB. This was studied with SEM and X-ray diffraction (XRD) showing a phase-pure deposition of the catalyst.

2. Results and discussion

2.1. Diamond Black fabrication

Developing materials with larger surface area is a common strategy when designing electrodes for electrochemical conversion reactions to obtain higher product yield by increasing the number of binding sites for reactants. Apart from that, enlarging the surface area leads to an increase in the capacitive current, which makes it particularly interesting for supercapacitor electrodes. For BDD, which inherently possesses a low capacitance,^[27] this was used in the past either through bottom-up or top-down approaches to develop more robust supercapacitors.^[28] The former using mainly templated growth methods, e.g., coating of silica beads, silicon nanowires, or quartz fibers,^[29–32] the latter employing masked surfaces and etching.^[24]

For this study, we chose BDD at a dopant concentration of $\sim 10^{21}$ cm⁻³ that is characterized by a low resistivity of 0.005 Ω cm and by a reversible behavior in CV almost independent from surface termination.^[13] Typically 5 μm thick diamond films were grown by CVD, resulting in crystallite sizes in the micron range. To make an electric connection to the diamond film without further processing, e.g., metal evaporation, the film was directly grown on conductive silicon wafers, seeded with detonation nanodiamonds (diameter ~ 4 nm). After growth, a few nanometer thick nickel layer was evaporated onto the surface and subsequently dewetted using rapid thermal annealing (RTA). From this process, a homogeneously covered diamond surface is obtained with nickel nanoparticles below 50 nm diameter (Figure 1a). The diamond film is then etched in an oxygen plasma resulting in a dark black diamond-coated wafer (Figure 1b). Very low content of sp² carbon is detected by XPS (Figure S1), and the G-peak usually associated with sp² carbon is not observed in Raman measurements, neither before nor after acid cleaning of the DB (Figure S2). Therefore, the black color cannot be attributed to graphitic impurities. Similar to black silicon, we assume that the color is caused by forming an effective medium without sharp interface but continuously changing the refractive index that effectively decreases reflection.^[33] Thus, light is effectively trapped in the material.

Characterization by SEM shows a coral-like structure (Figure 1c,d) with the diamond grains still being distinguishable. As polycrystalline BDD has randomly orientated crystals, this indicates, that the etching process is independent from the crystal lattice planes. The surface structures are asymmetric with dimensions from hundreds of nanometers in one dimension and only few tens of nanometers in the other. Typically, nanowires are obtained from top down etching as shown in literature before.^[24] However, for low plasma energies, also cylindrical structures have been observed.^[34] We assume that

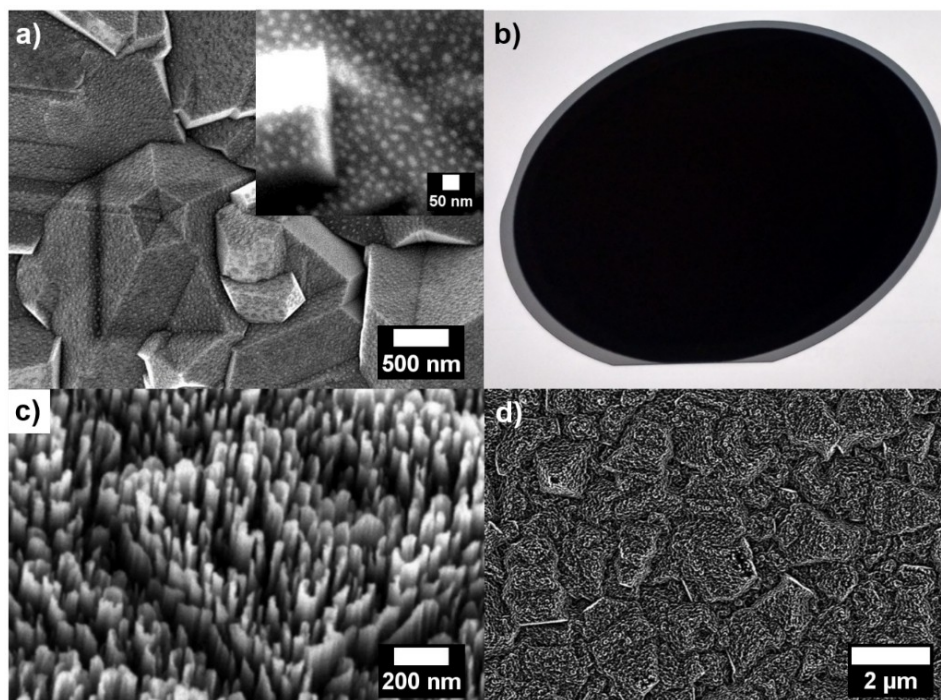


Figure 1. a) SEM of BDD covered with nanometer-sized nickel-droplets after dewetting by RTA (inset shows magnified view). b) Photograph of the 4" BDD coated wafer after top down etching showing the dark black color obtained from nanostructuring (gray boundary is the untreated diamond film that was covered by a clamping ring in the ICP-RIE). c) Zoomed in view of the coral-like nanostructure obtained and d) survey image showing the preservation of grain boundaries on the overall substrate.

our etching process is somewhere in between these two conditions. Another important aspect that should be taken into account is the high density of structural defects in heavily doped diamond, which may have an influence on the etching behavior.^[35] Indeed, we found that, as soon as the dopant concentration is decreased to 10^{20} cm^{-3} , the described process yields entirely different structures (Figure S3); however, a change in conductivity may also play a role. It is known that during growth depending on the crystal orientation the B-doping efficiency can vary strongly.^[36] However, for the used BDD films this variation does not result in different etching behavior as observed when comparing Figure 1a, c, and d. All crystal facets show the same structure. In the used BDD growth, a nanodiamond seed layer initially exposes a large amount of crystal orientations and growth will proceed mainly along the fastest growth direction, which should also result in lower dopant density variation compared to epitaxial growth on single crystal substrates.

Regarding a cross-sectional view of the structured film, an etch depth of approximately 200 nm is observed for the used conditions (Figure 2a). Longer etching times may be used to increase the depth, however, degradation of the mask material and changes in structure need to be taken into account. The lateral dimensions are below 50 nm and sidewall distance is smaller than 30 nm. After RIE, the structured sample is cleaned in boiling mixed acid (HNO_3 and H_2SO_4), which leaves the surface O-terminated. In this state, the electrode shows a complete wetting for aqueous solutions (Figure 2b). After

hydrogenating the surface by a plasma treatment, superhydrophobicity is observed (Figure 2c) by measuring the contact angle to 110° .

2.2. Electrochemical material characterization

CV was used to characterize the capacitance of manufactured DB with H- and O-termination in 1 M KCl solution. Using unstructured material from the same batch, reference data was obtained. The wetting behavior is entirely different for the different surface terminations; this is also reflected in the capacitive currents recorded. The H-terminated DB shows constant capacitance values of $43 \mu\text{F cm}^{-2}$, which is 7 times higher than an unstructured diamond film ($6.5 \mu\text{F cm}^{-2}$), the O-terminated DB results in a capacitance of $528 \mu\text{F cm}^{-2}$ (at 25 mVs^{-1}) and hence an approx. 80-fold increase (Figure 3a). The increased surface area obtained by the nanostructuring results in higher capacitance for both terminations compared to the unstructured films. In the case of DB, H-termination by H_2 -plasma does not change the surface morphology but leaves the surface hydrophobic. Thus, the electrolyte solution does not wet the entire surface, effectively decreasing the reachable surface area and the capacitance. For the O-terminated DB, the surface is fully wetted (see also Figure 2 b and c). The values are in good agreement with literature data, e.g., polycrystalline diamond films with a doping level of $3 \cdot 10^{20} \text{ cm}^{-3}$ resulted in a capacity of $6 \mu\text{F cm}^{-2}$,^[37] and heavily doped films ($4 \cdot 10^{21} \text{ cm}^{-3}$)

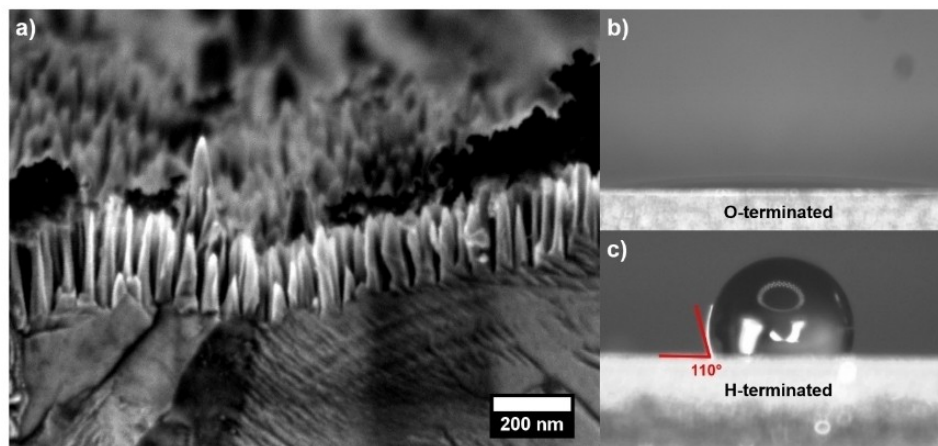


Figure 2. a) SEM cross-sectional view of DB showing the structural depth of approx. 200 nm. Contact angle measurements of b) O-terminated DB and c) H-terminated DB.

showed values around $8 \mu\text{F cm}^{-2}$.^[38] Single crystalline electrodes were reported with capacitance values as low as $3 \mu\text{F cm}^{-2}$.^[39] In the case of the nanostructured diamond, literature values up to $2800 \mu\text{F cm}^{-2}$ are reached using a combination of dry-etched template and overgrowth,^[40] a nanowire electrode obtained from overgrown black silicon reached $638 \mu\text{F cm}^{-2}$.^[41] The DB electrodes reach slightly lower values, however, employing polycrystalline diamond as substrate in contrast to (ultra-) nanocrystalline overgrowth. Regarding the kinetic behavior, it is observed that the O-terminated DB shows a decrease in capacitance at higher scan rates, e.g., $286 \mu\text{F cm}^{-2}$ at 100 mVs^{-1} . This is related to hindered diffusion into and from the nanoscopic trenches of the structures. Additionally, the CVs without redox mediator show no faradaic current peaks, which indicates that the nickel mask used for RIE was entirely removed (see also Figure 3b).

Scanning a larger potential range, after RIE, the redox peaks of surface-bound Ni (peak 2) are clearly visible at around 0.75 V (peak separation of 20 mV, non-reversible, Figure 3b). Cleaning the surface in mixed acid, the Ni is entirely removed as both peaks disappear. The O-terminated DB shows a small peak at around 1.1 V, which could be related to surface graphitization.^[42] However, as stated before, Raman and XPS measurements did not show any graphitic carbon (see Figures S1 and S2). For the H-terminated DB a large cathodic peak is observed in the first cycle at around 0.7 V (peak 3). This peak is still present in the following cycles but decreases in magnitude. When adding a redox mediator (peak 1), both surface terminations show comparable results with similar peak currents in the range of 0.15 mA cm^{-2} for a scan rate of 25 mVs^{-1} and 0.3 mA cm^{-2} at 100 mVs^{-1} (Figure 3b). Peak separation in both cases is close to 56 mV that indicates reversible behavior as also observed for the unstructured diamond electrode (data not shown). For the O-terminated DB an increase by 2 mV is observed at 100 mVs^{-1} . Here, for higher scan rates lower electron transfer kinetics will result in a further increased peak separation. Influence of surface termination on electron transfer kinetics for several redox mediators is well

described in literature, however, also highly depending on the used diamond quality.^[13,43] The nanostructuring in this case does not influence this behavior. Due to the high doping level of the used BDD, resulting in metallic conduction and possible non-diamond carbon content on the surface, the CV is still close to reversible. Peak separation values of around 60 mV on O-terminated diamond in ferro-/ferricyanide were also observed by Watanabe et al. at a doping level of $4 \text{ to } 5.5 \cdot 10^{21} \text{ cm}^{-3}$.^[38] The observed peak currents show that redox currents for all electrodes are diffusion limited (Figure 3c).

It is important to note, that the CVs shown in Figure 3b were recorded in as-prepared solutions (containing dissolved oxygen). Having a closer look on the H-terminated DB measurement, it is observable, that the overall CV is shifted to cathodic currents. This is only visible if the solution has not been degassed. In deoxygenated solutions, the CV of H-terminated DB is neither shifted to cathodic currents nor a peak at 0.7 V is observed (Figure S5). For the latter, however, this holds only true if the potential window is small enough to avoid water splitting and hence oxygen generation on the electrode surface. If oxygen is generated, the cathodic peak appears and a shift to cathodic currents is observed. From these observations, we assume that the H-terminated diamond surface is unstable in oxygenated solutions under open-circuit conditions and starts to oxidize as the oxygen reaches the surface. The instability of H-terminated diamond surfaces is known from literature,^[45] and here, we are able to observe it in electrochemical measurements on a nanostructured diamond electrode.

2.3. XPS material characterization

To get more insight into the role of surface termination on the DB-water interface, XPS at NAP conditions of water vapor was conducted at the synchrotron radiation facility BESSY II. In such conditions, the DB samples are excited with X-rays while being exposed to water molecules.

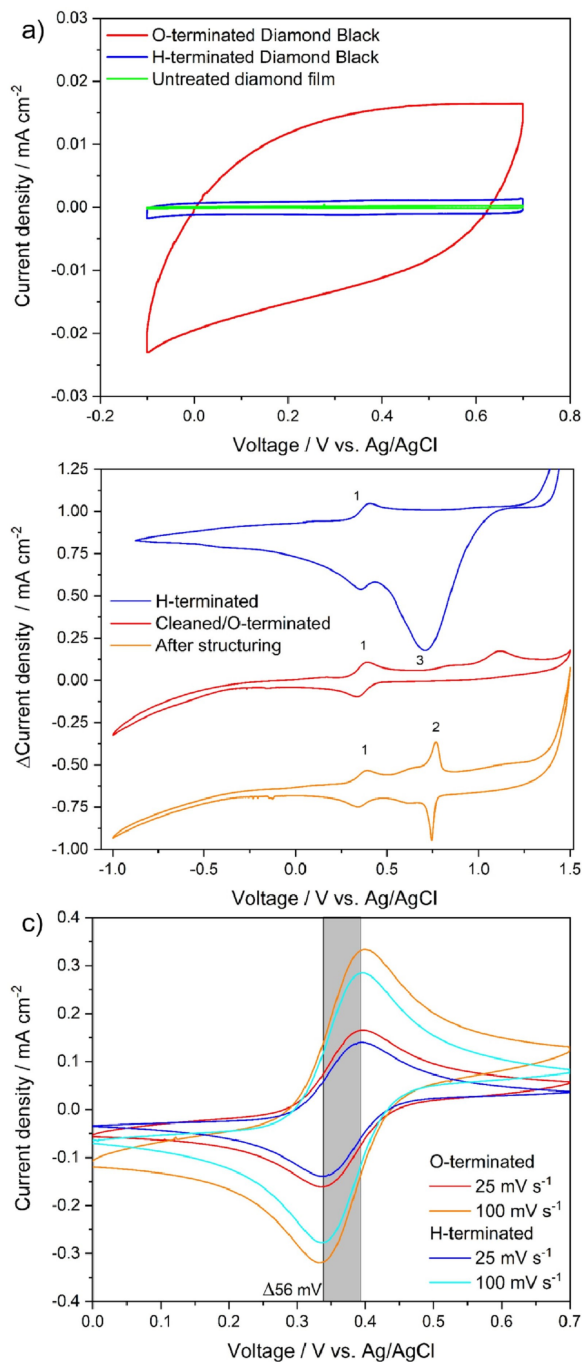


Figure 3. a) CV characterization in 1 M KCl solution showing significantly higher capacitive currents for the oxygen-terminated DB and non-linear behavior in relation to scan rate (inset compares current density at 0.6 V). b) CV characterization 1 mM $K_{3/4}[Fe^{II}/Fe^{III}(CN)_6]/1$ M KCl of the DB before and after surface treatments at larger potential windows in freshly prepared, not degassed solution (peaks: 1: redox mediator, 2: Ni, 3: surface oxidation). c) CV characterization in 1 mM $K_{3/4}[Fe^{II}/Fe^{III}(CN)_6]/1$ M KCl of O- and H-terminated DB at small potential window (peak separation of 56 mV indicated by gray area).

In Figure 4, the C1s and O1s spectra measured for O- and H-terminated DB samples are shown in vacuum (10^{-5} mbar) and NAP (2–4 mbar) of water vapor. The spectra were recorded with 600 eV and 850 eV excitation energies, respectively, to ensure a

mean free path of the photoelectrons below 2 nm and hence a high surface sensitivity.^[46] Even though the DB is a nanostructured electrode with nanoscale pores, almost complete hydrogen termination using an H_2 -plasma at 750 °C is readily achieved and no trace of sp^2 is detected with 600 eV excitation energy as opposed to lab-based measurements (Figure S1).

C1s XPS measurements show no significant changes for the O-terminated surface between the vacuum and the near-ambient pressure measurements. However, for H-terminated DB, a strong increase of the peak at 285.65 eV is observed after exposure to water (Figure 4a and Figure S6), which is attributed to C–O bonds, mostly from hydroxyl groups. An increase of the C=O bonds contribution is also observed in the range 286–290 eV (Table S2). We attribute the appearance of these peaks to the surface oxidation of H-terminated DB surface under X-ray illumination in the presence of water. The relative area of the C–O bonds contribution approximately doubles compared to vacuum conditions. Spectral changes were already detected from the first recorded XPS spectra and remained stable over time. A spontaneous water dissociation upon water exposure is not probable as the samples characterized in vacuum have been previously exposed to ambient air and demonstrate a low surface oxidation. A photochemical reaction, induced by the X-rays, occurring rapidly after illumination (< 20 seconds) is therefore probable.

At the oxygen core level, a strong peak at 535 eV appears in NAP condition (Figure 4b), which is the signature of water molecules in the vapor phase. A relative increase of the peak at 531.5 eV is attributed to the formation of a liquid water film on the DB surface. The other oxygen signatures are difficult to assign without theory support as the liquid water signal is strongly overlapping with the diamond surface oxygen species. Relative changes in the spectra may be related to different water thicknesses, which cannot be reliably measured *in situ*.

From the XPS measurements performed under water atmosphere, we can conclude that the H-termination on DB is not stable in the presence of water upon X-ray irradiation, as opposed to oxygen terminations. We assume that the high energy radiation (> 100 eV) leads to radiolysis of water forming different radical species close to the DB surface.^[47] The radical species may also be a result of the emission of secondary electrons from the H-terminated DB, as previously reported for hydrogenated nanodiamonds.^[48,49] As shown in the electrochemical characterization, the H-terminated DB surface is readily oxidized in the presence of reactive species. Most likely, chemical reactions with hydroxyl radicals lead first to a surface hydroxylation, which was also observed on nanodiamonds exposed to UV light in the presence of water.^[50] Subsequently, due to condensation, ether and carbonyl groups can be formed at the surface.^[51] Although the surface oxidation of H-terminated diamond has been previously reported,^[45] to the best of our knowledge, it has never been directly observed *in situ* before. We assume that the increased surface area of DB increases the detectable signal and hence the sensitivity, which makes the measurement of the surface oxidation possible. Note that for a higher X-ray excitation energy (1200 eV), the similar spectral change at the C1s under water exposure is observed

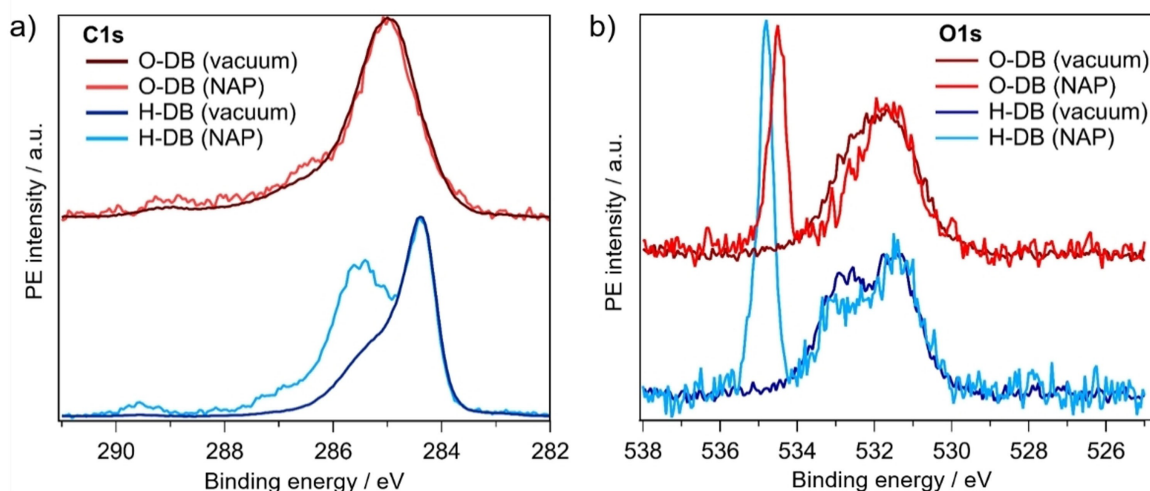


Figure 4. a) C1s and b) O1s XPS of DB under vacuum (10^{-5} mbar) and near ambient pressure of water ($\sim 2\text{--}4$ mbar) with hydrogenated (blue) and oxidized (red) surfaces. The excitation energy was 600 eV and 850 eV for C1s and O1s, respectively. The spectra are normalized to their maximum (excluding the gas phase contribution for O1s).

but with much lower intensity, showing that surface-sensitive XPS is highly relevant in this case (Figure S6). Apart from that, due to the nanostructuring, an increased reactivity is expected as previously observed for nanodiamonds and other nanomaterials.^[52,53]

2.4. CO₂ reduction using Diamond Black

For photoelectrochemical reactions, apart from strong light absorption and stability, surface area and reactivity play an important role.^[54] Thus, DB is a highly interesting material in this field. Due to the large band gap, direct photo-excitation is only possible with high energy UV light. Using suitable materials like cuprous oxide (Cu₂O), light absorption in the visible spectrum can be achieved, paired with an electrocatalytic effect and increased product selectivity due to the improved surface chemical activity of a catalytic material such as Cu₂O in comparison to the chemically inert diamond surface.^[21,55] This material is effectively incorporated on the electrodes surface by a galvanostatic deposition in a basic aqueous copper(II) sulfate solution containing lactic acid at elevated temperatures.^[56]

Interestingly, the morphology and deposition efficiency of Cu₂O on DB depends on the surface termination. On an O-terminated DB 100-face, cubes (lowest surface energy) are formed at high growth rates (Figure 5a and d). On H-terminated DB, 111-face particles are obtained at low growth rates forming truncated polyhedral structures (Figure 5b). Due to the high deposition rate, an almost complete coverage is already obtained after 60 s (Figure 5c). The surface termination also strongly influences the amount of nucleation sites and hence the overall size distribution of the deposited particles (Figure S7). The purity of Cu₂O deposited electrodes was confirmed by XPS analysis and XRD (Figure S8, S9). This is important as catalytic activity and product selectivity in CO₂ reduction is

strongly affected by morphology, orientation, shape, and grain size of Cu₂O deposited films. From literature it is known that, e.g., cubic-shaped particles have higher selectivity to form CO, CH₄ and ethanol.^[57] Also, crystallite size influences faradaic efficiency of e.g., ethylene production.^[58] For a detailed study of the photoelectrochemical reduction of CO₂ to liquid products on these electrodes, we have chosen different deposition times that do not entirely cover the surface (from 1 to 30s) on both, H- and O-terminated DB.

An important aspect for the reduction of CO₂ in liquid electrolytes is the solubility of the gas in the used media. For this study, we have chosen an ammonium-based RTIL, Butyltrimethylammonium bis-trifluorosulfonimide (N₁₁₁₄ BTA), which is known to have a high CO₂ solubility.^[25] Apart from that ammonium RTILs often benefit from improved electrochemical and photochemical stability, i.e., larger potential window (up to 6 V for N₁₁₁₄ BTA), reduced overpotentials, and low vapor pressure.^[59] However, they are only useful for photoelectrochemistry if thermal- and photostability is sufficient as well as viscosity is appropriate for the used application. To provide protons in the solution enabling the formation of e.g., methanol, ethanol, or formic acid, 1 M of water was added and the IL was mixed 3:1 with dimethylsulfoxide (DMSO) in order to further reduce the viscosity and enhance transport properties of the electrolyte.

The DB photocatalytic performance was studied in the presence of CO₂ (continuously bubbled in the solution). It was found that formate was the main and predominant product of the CO₂ reduction reaction with a faradaic efficiency of 50–70% for the Cu₂O-modified electrodes. The flat band potential of the Cu₂O/BDD interface has been measured to be 0.75 V vs. reversible hydrogen electrode (RHE) in aqueous media.^[60] The flat band potential is considered to be a close approximation of the valence band edges in p-type semiconductors such as Cu₂O,^[61] therefore the conduction band edge can be easily

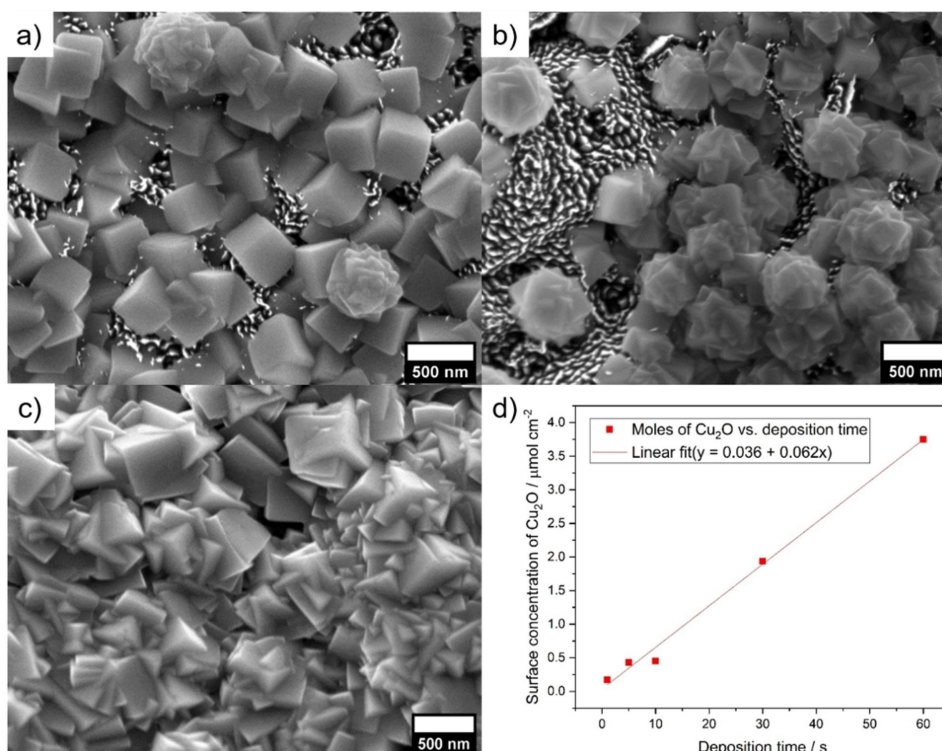


Figure 5. Deposition of Cu_2O on DB electrodes with different termination: a) SEM of O-DB after 30s deposition showing a cubic morphology with 100-face, b) H-DB after 30s deposition resulting in truncated polyhedra with 111-face, and c) 60 s deposition on H-DB showing an almost entirely coated diamond surface. d) Surface Cu_2O concentration as a function of deposition time on O-DB.

calculated from the optical band gap of Cu_2O (2.17 eV). This leads to a value of -1.42 V vs. RHE for the conduction band edge of Cu_2O . This is sufficiently negative for the photoelectrochemical reduction of CO_2 to a product such as formic acid for which the reduction potential is -0.61 V vs. RHE.

For this reason, we focused our investigations on the determination of formate for evaluating the electrode performance. Apart from formate, in aqueous media, traces of methanol, ethanol, and acetone were found. Gaseous products were not taken into account so far, as accurate quantification is rather challenging. The best performing electrode was an O-terminated DB with 30s Cu_2O deposition reaching a formate yield of $14 \mu\text{mol cm}^{-2} \text{h}^{-1}$ (see Figure 5a, Figure 6a and Table 1), the H-terminated DB yields 30% less formate using the same deposition time. From Figure 6a it is observable, that the O-terminated diamond results in higher current densities especially in the first 30 minutes. As there is no change in wettability for the terminations when using ILs, this is most likely caused by a lower coverage with Cu_2O resulting from the lower deposition rate at H-terminated DB. This trend is also visible for the illuminated catalyst when focusing on the first three minutes (see Figure 6a, inset). However, in this stage and without illumination, the H-DB, after equilibration, shows higher current densities which could be explained by faster reduction of the Cu_2O on the surface. Without the use of Cu_2O as co-catalyst, only formate yields below $0.1 \mu\text{mol cm}^{-2} \text{h}^{-1}$ were obtained. With a deposition time of only one second for the DB

Table 1. Formic acid production rates in $\mu\text{mol cm}^{-2} \text{h}^{-1}$ and Faradaic efficiencies at variously treated diamond electrodes. Electrolyte: 3:1 N_{1114} BTA : DMSO with 1 M H_2O . Applied potential: -1.7 V vs. Ag/AgCl.

Electrode	Illumination	Formate yield [$\mu\text{mol cm}^{-2} \text{h}^{-1}$]	Faradaic Efficiency [%]
O-DB blank	Sun	0.08	9.2
H-DB blank	Sun	0.07	10.3
Cu_2O O-DB, 1.0 s	Sun	6.07	67.0
Cu_2O O-DB, 1.0 s	dark	4.07	55.6
Cu_2O H-DB, 1.0 s	Sun	7.10	65.1
Cu_2O H-DB, 1.0 s	dark	2.88	50.1
Cu_2O O-DB, 5.0 s	Sun	8.41	72.0
Cu_2O H-DB, 5.0 s	Sun	8.18	62.3
Cu_2O O-DB, 30 s	Sun	14.05	68.1
Cu_2O O-DB, 30 s	dark	11.07	69.7
Cu_2O H-DB, 30 s	Sun	9.73	64.7
Cu_2O H-DB, 30 s	dark	6.82	60.6
Cu_2O O-EG-BDD, 5.0 s	Sun	3.93	58.3
Cu_2O O-EG-BDD, 1.0 s	Sun	1.17	42.0

electrodes, the increase in formate yield due to illumination was 30% for the O-DB and 59% for the H-DB. Using 30 s deposition time an overall increase of approx. 30% was obtained for both surface terminations. An overview of all CO_2 reduction reactions is shown in Table 1.

For comparison, DB and polycrystalline BDD electrodes were also studied in aqueous 0.5 M KHCO_3 . Here, however, only formate yields below $0.7 \mu\text{mol cm}^{-2} \text{h}^{-1}$ for Cu_2O on O-DB and $0.1 \mu\text{mol cm}^{-2} \text{h}^{-1}$ for blank DB were obtained, which can be explained by the significantly lower CO_2 uptake of the electro-

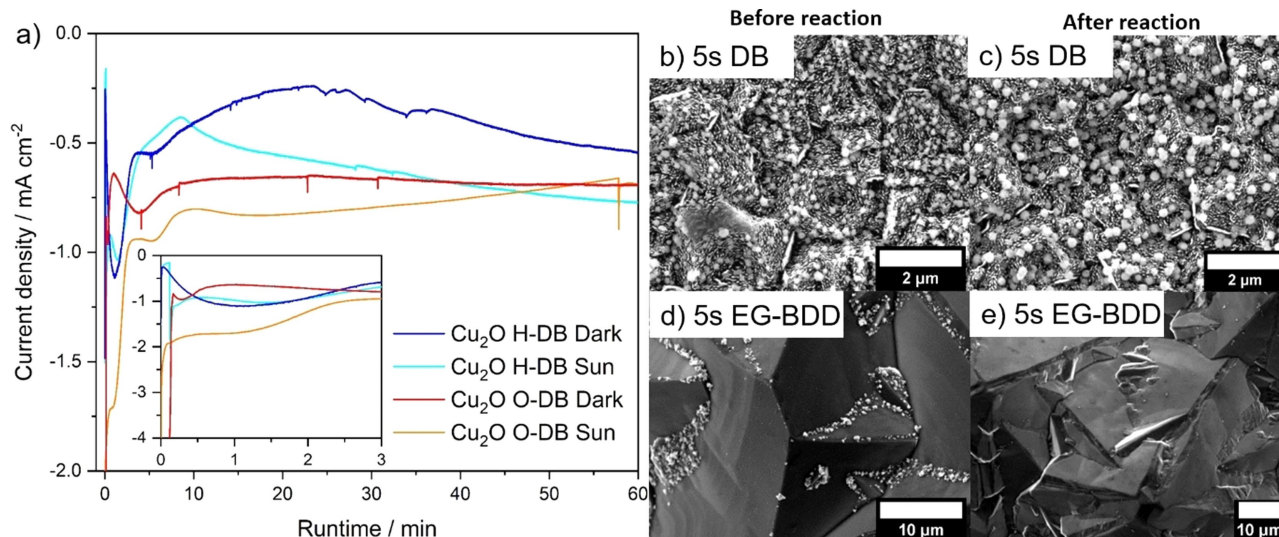


Figure 6. a) Photoelectrochemical CO_2 conversion on Cu_2O -decorated DB electrodes (deposition time 30 s) with and without illumination from a solar simulator at -1.7 V vs Ag/AgCl in 3:1 N_{1114} BTA : DMSO with 1 M H_2O (inset shows initial 3 minutes). b) SEM of DB electrode decorated with Cu_2O (5 s deposition time) before and c) after CO_2 conversion experiment. d) EG-BDD decorated with Cu_2O (5 s deposition time) before and e) after CO_2 conversion.

lyte. Apart from that, depositions on electrochemical grade diamond (EG-BDD, Element6) and on DB have been carried out. It was found that for DB, the deposition rate is higher, i.e., high coverage is obtained after only a few seconds of deposition. Apart from the high surface reactivity, this may be explained by a higher dopant concentration in the DB electrodes. In addition, whereas the EG-BDD electrode shows mainly deposition close to grain boundaries and hence large parts of the electrode surface are not covered, the DB reveals a more homogeneous distribution of the Cu_2O particles (Figure 6b, d).

Comparing EG-BDD with DB electrodes, it is observed that for EG-BDD at low deposition time of 1 s, an approximately 6 times lower formate yield is achieved. In addition, when studying the morphology and the surface coverage of electrodes before and after reaction by SEM and XPS analysis (Figure 6b-e and Figure S8), it is clearly visible that the Cu_2O particles are strongly adhering to the DB films and conserve their shape, whereas for the EG-BDD almost no Cu_2O can be found anymore. Due to the almost inert surface of diamond, catalyst adhesion on BDD electrodes has always been a major issue for long-term processes.^[11] Using the fine nanostructure of DB, we assume that we can achieve stronger adhesion by increasing the interfacial area of the deposited catalyst particles with the electrode.

4. Conclusion

For photoelectrochemical applications, the fabrication of heavily nanostructured diamond electrodes offers several advantages like increased surface area and light trapping. For heavily B-doped polycrystalline films, a top-down structuring approach can result in nanoscale structures homogeneously distributed over the whole film, which cause a dark black color of the

substrate. These so-called *Diamond Black* electrodes show increased surface reactivity towards oxidation when H-terminated. *In situ* surface oxidation of H-terminated DB in the presence of water vapor is demonstrated using NAP-XPS, which is not observed for O-terminated DB. In accordance with this measurement, surface oxidation is observed in CV measurements. In addition, we demonstrate that the deposition of phase pure Cu_2O catalyst materials on nanostructured DB electrode can be controlled through the surface termination. In comparison to unstructured BDD electrodes, better nucleation and surface coverage was obtained. Such electrodes are versatile photocathodes in CO_2 reduction reactions with an increased long-term stability as observed for Cu_2O deposits. Due to the high surface reactivity, DB reaches high formate yields already at low catalyst deposition times. The produced formate is a green fuel that can be used e.g., for fuel cells.^[62] Additionally, DB is not only promising in CO_2 conversion but also for other (photo)electrochemical processes, e.g., in sensing devices due to an improved surface adhesion and an increased surface area.

Experimental section

Sample preparation: Heavily boron doped diamond layers on silicon were manufactured following a procedure described elsewhere.^[63,64] Briefly, 0.01–0.02 Ωcm silicon wafers (Si-Mat, Germany) were seeded with hydrogen-terminated nanodiamonds (G01 grade, Plasmachem GmbH, Germany) in 10^{-3} M KCl aqueous solution. After a dip in ultrapure water and spin drying, the wafers were loaded into the diamond reactor.

An ellipsoidal microwave plasma chemical vapor deposition (MPCVD) (915 MHz) reactor with purified gases (hydrogen, methane, and trimethylborane (TMB)) was employed for boron doped diamond growth.^[65] Identical growth conditions were used

for all films: 9 kW microwave power, 750 °C substrate temperature, 50 mbar pressure, 2% methane in H₂, and a TMB concentration of 2000 ppm. The typical growth thickness for the electrodes used in CO₂ reduction was 5 μm. For additional characterization, an additional film with 20 μm thickness was grown that showed the same properties in terms of RIE structuring and electrochemical response. The obtained films contain approx. 10²¹ B/cm³ as determined by secondary ion mass spectrometry (SIMS).^[66] Further processing was carried out on the as-grown diamond.

The boron doped polycrystalline diamond (BDD) was then patterned top down using inductively coupled-reactive ion etching (ICP-RIE) and a mask of Ni nanodroplets obtained from dewetting via rapid thermal annealing (RTA). The process was adapted from an approach we previously developed for obtaining high-aspect diamond nanowires.^[24] A ~2 nm Ni film was deposited onto the BDD that is subsequently dewetted by RTA at 850 °C for 1 min forming 20–60 nm metal droplets. 3 nm Ni layers gave droplets of up to 130 nm (Figure S4). After ICP-RIE in an oxygen plasma for 4 min, a dark black diamond layer is obtained. Etching parameters were as follows: 30 sccm O₂ with 700 W ICP power, 300 W platen power at 1.3 Pa, resulting in a bias of approx. –350 V.

In order to remove the Ni etch mask the wafers are thoroughly cleaned in a mixture of sulfuric and nitric acid (ratio 3:1) for 1.5 h at elevated temperatures. Apart from the mask removal, this procedure decreases graphitic contents and results in an O-terminated surface. Surface hydrogenation was carried out in an H₂-plasma at 750 °C for 30 min in the MPCVD reactors. Directly after the termination steps, possible changes in the diamond crystal structure or boron concentration of the nanostructured BDD was characterized by Raman spectroscopy using a laser wavelength of 532 nm (InVia, Renishaw, UK), the morphology was investigated by scanning electron microscopy, and the wetting properties were measured by contact angle measurements.

Electrochemical material characterization: Characterizations were carried out with a BioLogic potentiostat (VMP3, BioLogic Science Instruments, France) using a custom electrochemical cell equipped with an Ag/AgCl (3 M KCl) as reference and a platinum counter electrode (all potentials reported in this study are reported against the used reference electrode). The diamond film electrode was mounted in the cell and electrical contact was established by the silicon substrate. Cyclic voltammetry (CV) was carried out either with as-prepared (to study the influence of dissolved oxygen) or degassed solutions of 1 M KCl without added redox mediator, with 1 mM K₃/4[Fe^{II}/Fe^{III}(CN)₆], or with 1 mM [Ru(NH₃)₆]Cl₃ (all chemicals obtained from Sigma Aldrich, Germany).

Near-ambient pressure XPS

The XPS spectroscopic measurements were carried out at the U49/2-PGM-1 beamline at the synchrotron radiation facility BESSY II in Berlin, Germany,^[67] using the near-ambient pressure Sol³PES experimental setup, which is equipped with a Scienta Omicron R4000 HIP-2 hemispherical electron analyzer.^[68] There are three differential pumping sections, each consisting of a pinhole and two turbo molecular pumps, to separate the detector unit from the experimental chamber. A similar differential pumping scheme is used to deal with the pressure difference between the experimental chamber and the ultra-high vacuum (<10⁻⁹ mbar) inside the beamline. During our measurements the angle between the polarization axis of the incoming soft X-ray and the electron analyzer was 54.7° (magic-angle geometry) to avoid any photoelectron angular distribution effects. PE measurements were performed at high vacuum (between 8×10⁻⁵ and 6×10⁻⁶ mbar) and NAP conditions (between 2 and 4 mbar). The distance between the

electron analyzer entrance pinhole and the focal point of the soft X-ray beam was shorter than 500 μm, minimizing electron scattering at elevated water vapor pressure in the chamber that causes an attenuated electron signal. To create the water vapor environment we connected a test tube filled with ultrapure water (degassed by two freeze-pump-thaw cycles) to the vacuum chamber. A needle valve was used to set the required H₂O gas flow into the chamber. The pumping flow rate is controlled with a motorized gas-regulating valve (Pfeiffer EVR 116), which was managed by a proportional-integral-derivative controller (Pfeiffer RVC300 pressure gauge). Additionally, a temperature-controlled chiller (Julabo F12-ED) actively cooled our sample holder. The U49/2 beamline provides high-brilliant soft X-ray light up to a photon energy of E_{ph}=1400 eV, enough to core-ionize oxygen and carbon. The energy resolution of the beamline was better than 75 meV at 600 eV, and ~350 meV at 1200 eV photon energy. The energy resolution of the electron analyzer was 250 meV for our measurements at low kinetic energies (i.e. at 600 eV photon energy, pass energy of 100 eV), and 500 meV for measurements at high kinetic energies (i.e. at 1200 eV photon energy, pass energy of 200 eV). The recorded C1s and O1s spectra were energy-calibrated against the Fermi edge, which was measured separately after each scan.

Cu₂O deposition and characterization: Cuprous oxide promoted diamond electrodes were prepared by depositing Cu₂O onto clean EG-BDD and DB wafers by a galvanostatic method, with various deposition times, 60, 30, 5 and 1 s. The aqueous solution of 1.5 M lactic acid and 0.2 M CuSO₄ was used and pH adjusted to 12.5 with NaOH. During deposition, the solution was kept at 65 °C, while the deposition current was held at –6.6 mA (vs. Ag/AgCl). Surface coverage and morphology of the as received and Cu₂O deposited samples before and after CO₂ reduction reaction were investigated as a function of deposition time by XPS and SEM techniques. The surfaces were prepared with H or O termination and studied by XPS. The composition of samples was also examined by XPS using an Al K_α (hν=1486.6 eV) X-ray source operated in the constant analyzer energy mode with a 400 microns spot size. Data analysis was performed in CasaXPS software. The SEM images of the modified electrodes were taken with a JEOL-6500F scanning electron microscope with an acceleration voltage of 10 kV.

Photocatalytic experiments: The photoelectrocatalytic performance of solid O and H terminated DB wafers fixed in epoxy (to cover Si back side) as well as polycrystalline BDD were investigated. The photoelectrocatalytic experiments were performed using chronoamperometry with μ-Autolab potentiostat/galvanostat (Ecochemie, NL) in a single pot reactor, with a three-electrode setup using Ag/AgCl (1 M KCl) as a reference electrode.

The photoelectrocatalytic performance of various diamond cathodes was tested at –1.2 V and –1.7 V in 0.5 M KHCO_{3(aq)}, and in 3:1 N₁₁₁₄ BTA:DMSO containing 1 M H₂O, respectively (N₁₁₁₄ BTA, purity 99.5%, was provided by IOLITEC, Germany). The reference electrode used in all these measurements was Ag/AgCl (1 M KCl). Water was added to the reaction IL mixture to provide a source of protons and hence enabling the formation of protonated CO₂ reduction products. Sample irradiation was performed with a commercial solar simulator (1 Sun 100 mW/m²) based on a Xe lamp and filters. Liquid samples were extracted from the reaction volume and subsequently analyzed by ¹H NMR. For analyzing the liquid products from KHCO_{3(aq)} experiments 4,4-dimethyl-4-silapentane-1-sulfonic acid (DSS) was used as an internal standard, while for ionic liquids a new protocol was developed based on a reference standard of formic acid in 3:1 N₁₁₁₄ BTA:DMSO.

Acknowledgements

This work was supported by European Union's Horizon 2020 Research and Innovation program under Grant no. 665085 (DIACAT). R.S. acknowledges an Emmy Noether Young Investigator stipend through the German Research Foundation (project SE 2253/3-1). Open access funding enabled and organized by Projekt DEAL.

Conflict of Interest

The authors declare no conflict of interest.

Keywords: nanostructures · electrocatalysts · carbon dioxide chemistry · ionic liquids · near ambient pressure XPS

- [1] European Parliament, *P9_TA(2019)0078* **2019**, 78–79.
- [2] P. P. Tans, I. Y. Fung, T. Takahashi, *Science* **1990**, *247*, 1431–1438.
- [3] S. Manabe, R. T. Wetherald, *J. Atmos. Sci.* **1980**, *37*, 99–118.
- [4] C. Falter, V. Batteiger, A. Sizmann, *Environ. Sci. Technol.* **2016**, *50*, 470–477.
- [5] F. S. Zeman, D. W. Keith, *Philos. Trans. R. Soc. London* **2008**, *366*, 3901–3918.
- [6] R. J. Lim, M. Xie, M. A. Sk, J. M. Lee, A. Fisher, X. Wang, K. H. Lim, *Catal. Today* **2014**, *233*, 169–180.
- [7] A. Corma, H. Garcia, *J. Catal.* **2013**, *308*, 168–175.
- [8] Q. Lu, F. Jiao, *Nano Energy* **2016**, *29*, 439–456.
- [9] J. Wu, Y. Huang, W. Ye, Y. Li, *Adv. Sci.* **2017**, *4*, 1–29.
- [10] N. N. Vu, S. Kaliaguine, T. O. Do, *Adv. Funct. Mater.* **2019**, *29*, 1–44.
- [11] M. Ma, K. Liu, J. Shen, R. Kas, W. A. Smith, *ACS Energy Lett.* **2018**, *3*, 1301–1306.
- [12] C. W. Li, M. W. Kanan, *J. Am. Chem. Soc.* **2012**, *134*, 7231–7234.
- [13] J. V. Macpherson, *Phys. Chem. Chem. Phys.* **2015**, *17*, 2935–2949.
- [14] S. J. Cobb, Z. J. Ayres, J. V. Macpherson, *Annu. Rev. Anal. Chem.* **2018**, *11*, 463–484.
- [15] D. Zhu, L. Zhang, R. E. Ruther, R. J. Hamers, *Nat. Mater.* **2013**, *12*, 836–841.
- [16] V. Chakrapani, J. C. Angus, A. B. Anderson, S. D. Wolter, B. R. Stoner, G. U. Sumanasekera, *Science* **2007**, *318*, 1424–1430.
- [17] S. Choudhury, B. Kiendl, J. Ren, F. Gao, P. Knittel, C. Nebel, A. Venerosy, H. Girard, J.-C. Arnault, A. Krueger, K. Larsson, T. Petit, *J. Mater. Chem. A* **2018**, *6*, 16645–16654.
- [18] N. Roy, Y. Hirano, H. Kuriyama, P. Sudhagar, N. Suzuki, K. Katsumata, K. Nakata, T. Kondo, M. Yuasa, I. Serizawa, T. Takayama, A. Kudo, A. Fujishima, C. Terashima, *Sci. Rep.* **2016**, *6*, 38010.
- [19] P. K. Jiwanti, K. Natsui, K. Nakata, Y. Einaga, *Electrochim. Acta* **2018**, *266*, 414–419.
- [20] E. Verlato, S. Barison, Y. Einaga, S. Fasolin, M. Musiani, L. Nasi, K. Natsui, F. Paolucci, G. Valenti, *J. Mater. Chem. A* **2019**, *7*, 17896–17905.
- [21] D. Denala, M. Khalil, T. A. Ivandini, 2019; Vol. 020057, p. 020057.
- [22] Z. Hubička, M. Zlámal, M. Čada, Š. Kment, J. Krýsa, *Catal. Today* **2019**, *328*, 29–34.
- [23] S. A. Yao, R. E. Ruther, L. Zhang, R. A. Franking, R. J. Hamers, J. F. Berry, *J. Am. Chem. Soc.* **2012**, *134*, 15632–15635.
- [24] W. Smirnov, A. Kriele, N. Yang, C. E. Nebel, *Diamond Relat. Mater.* **2010**, *19*, 186–189.
- [25] Z. Lei, C. Dai, B. Chen, *Chem. Rev.* **2014**, *114*, 1289–1326.
- [26] S. Xie, Q. Zhang, G. Liu, Y. Wang, *Chem. Commun.* **2016**, *52*, 35–59.
- [27] G. M. Swain, R. Ramesham, *Anal. Chem.* **1993**, *65*, 345–351.
- [28] F. Gao, C. E. Nebel, *ACS Appl. Mater. Interfaces* **2016**, *8*, 28244–28254.
- [29] P. Knittel, T. Yoshikawa, C. E. Nebel, *Anal. Chem.* **2019**, *91*, 5537–5541.
- [30] S. Ruffinatto, H. A. Girard, F. Becher, J. C. Arnault, D. Tromson, P. Bergonzo, *Diamond Relat. Mater.* **2015**, *55*, 123–130.
- [31] F. Gao, C. E. Nebel, *ACS Appl. Mater. Interfaces* **2016**, *8*, 18640–18646.
- [32] F. Gao, M. T. Wolfer, C. E. Nebel, *Carbon* **2014**, *80*, 833–840.
- [33] S. Koynov, M. S. Brandt, M. Stutzmann, *Appl. Phys. Lett.* **2006**, *88*.
- [34] W. Janssen, E. Gheeraert, *Diamond Relat. Mater.* **2011**, *20*, 389–394.
- [35] W. L. Wang, M. C. Polo, G. Sánchez, J. Cifre, J. Esteve, *J. Appl. Phys.* **1996**, *80*, 1846–1850.
- [36] R. Samlenski, C. Haug, R. Brenn, C. Wild, R. Locher, P. Koidl, *Diamond Relat. Mater.* **1996**, *5*, 947–951.
- [37] L. a Hutton, J. G. Iacobini, E. Bitziou, R. B. Channon, M. E. Newton, J. V. Macpherson, *Anal. Chem.* **2013**, *85*, 7230–7240.
- [38] T. Watanabe, T. K. Shimizu, Y. Tateyama, Y. Kim, M. Kawai, Y. Einaga, *Diamond Relat. Mater.* **2010**, *19*, 772–777.
- [39] A. Fujishima, Y. Einaga, T. N. Rao, D. A. Tryk, *Diamond Electrochemistry*; Elsevier Science, 2005.
- [40] T. Kondo, K. Yajima, T. Kato, M. Okano, C. Terashima, T. Aikawa, M. Hayase, M. Yuasa, *Diamond Relat. Mater.* **2017**, *72*, 13–19.
- [41] P. W. May, M. Clegg, T. A. Silva, H. Zanin, O. Fatibello-Filho, V. Celorrio, D. J. Fermin, C. C. Welch, G. Hazell, L. Fisher, A. Nobbs, B. Su, *J. Mater. Chem. B* **2016**, *4*, 5737–5746.
- [42] J. A. Bennett, J. Wang, Y. Show, G. M. Swain, *J. Electrochem. Soc.* **2004**, *151*, E306.
- [43] L. Kavan, Z. Vlckova Zivcova, V. Petrak, O. Frank, P. Janda, H. Tarabkova, M. Nesladek, V. Mortet, *Electrochim. Acta* **2015**, *179*, 626–636.
- [44] I. Yagi, H. Notsu, T. Kondo, D. A. Tryk, A. Fujishima, *J. Electroanal. Chem.* **1999**, *473*, 173–178.
- [45] P. E. Pehrsson, T. W. Mercer, J. A. Chaney, *Surf. Sci.* **2002**, *497*, 13–28.
- [46] M. P. Seah, W. A. Dench, *Surf. Interface Anal.* **1979**, *1*, 2.
- [47] S. Le Caër, *Water* **2011**, *3*, 235–253.
- [48] M. Kurzyp, H. A. Girard, Y. Cheref, E. Brun, C. Sicard-Roselli, S. Saada, J.-C. Arnault, *Chem. Commun.* **2017**, *53*, 1237–1240.
- [49] E. Brun, H. A. Girard, J.-C. Arnault, M. Mermoux, C. Sicard-Roselli, *Carbon* **2020**, *162*, 510–518.
- [50] H. A. Girard, T. Petit, S. Perruchas, T. Gacoin, C. Gesset, J. C. Arnault, P. Bergonzo, *Phys. Chem. Chem. Phys.* **2011**, *13*, 11517.
- [51] L. M. Struck, M. P. D'Evelyn, *J. Vac. Sci. Technol. A: Vacuum, Surfaces, and Films* **1993**, *11*, 1992–1997.
- [52] J. L. Gole, C. Burda, Z. L. Wang, M. White, *J. Phys. Chem. Solids* **2005**, *66*, 546–550.
- [53] O. A. Williams, J. Hees, C. Dieker, W. Jäger, L. Kirste, C. E. Nebel, *ACS Nano* **2010**, *4*, 4824–4830.
- [54] A. Rani, R. Reddy, U. Sharma, P. Mukherjee, P. Mishra, A. Kuila, L. C. Sim, P. Saravanan, *A review on the progress of nanostructure materials for energy harnessing and environmental remediation*; Springer Heidelberg, 2018; Vol. 8.
- [55] R. Kas, R. Kortlever, A. Milbrat, M. T. M. Koper, G. Mul, J. Baltrusaitis, *Phys. Chem. Chem. Phys.* **2014**, *16*, 12194–12201.
- [56] Y. C. Zhou, J. A. Switzer, *Mater. Res. Innovations* **1998**, *2*, 22–27.
- [57] J. Bugayong, G. L. Griffin, *ECS Trans.* **2013**, *58*, 81–89.
- [58] A. D. Handoko, C. W. Ong, Y. Huang, Z. G. Lee, L. Lin, G. B. Panetti, B. S. Yeo, *J. Phys. Chem. C* **2016**, *120*, 20058–20067.
- [59] H. Liu, Y. Liu, J. Li, *Phys. Chem. Chem. Phys.* **2010**, *12*, 1685.
- [60] C. K. Mavrokefalos, M. Hasan, J. F. Rohan, R. G. Compton, J. S. Foord, *Appl. Surf. Sci.* **2017**, *408*, 125–134.
- [61] J.-N. Nian, C.-C. Tsai, P.-C. Lin, H. Teng, *J. Electrochem. Soc.* **2009**, *156*, H567.
- [62] C. Rice, S. Ha, R. I. Masel, P. Waszczuk, A. Wieckowski, T. Barnard, *J. Power Sources* **2002**, *111*, 83–89.
- [63] T. Yoshikawa, V. Zuerbig, F. Gao, R. Hoffmann, C. E. Nebel, O. Ambacher, V. Lebedev, *Langmuir* **2015**, *31*, 5319–5325.
- [64] J. Hees, A. Kriele, O. A. Williams, *Chem. Phys. Lett.* **2011**, *509*, 12–15.
- [65] M. Fünser, C. Wild, P. Koidl, *Appl. Phys. Lett.* **1998**, *72*, 1149–1151.
- [66] S. Roscher, R. Hoffmann, M. Prescher, P. Knittel, O. Ambacher, *RSC Adv.* **2019**, *9*, 29305–29311.
- [67] K. J. S. Sawhney, F. Senf, W. Gudat, *Nucl. Instrum.* **2001**, *467–468*, 466–469.
- [68] R. Seidel, M. N. Pohl, H. Ali, B. Winter, E. F. Aziz, *Rev. Sci. Instrum.* **2017**, *88*, 073107.

Manuscript received: June 4, 2020

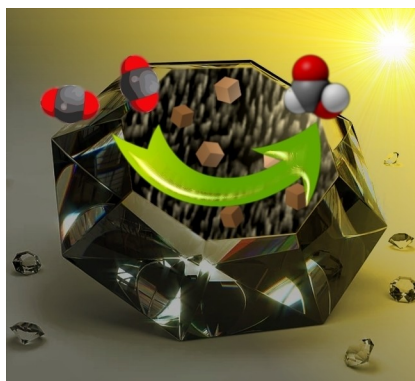
Revised manuscript received: July 28, 2020

Accepted manuscript online: August 5, 2020

Version of record online: ■■■, ■■■■

FULL PAPERS

A new best friend? A nanostructured boron doped diamond electrode with a 80-fold increased surface area is presented that shows higher surface reactivity in electrochemical characterization as well as near-ambient pressure X-ray photoelectron spectroscopy. CO₂ conversion to liquid products in room temperature ionic liquids with high efficiency and enhanced catalyst stability is obtained using these electrodes modified with Cu₂O.



Dr. P. Knittel, Dr. F. Buchner, Dr. E. Hadzifejzovic, Dr. C. Giese, P. Quellmalz, Dr. R. Seidel, Dr. T. Petit, Dr. B. Iliev, Dr. T. J. S. Schubert, Prof. C. E. Nebel, Prof. J. S. Foord*

1 – 11

Nanostructured Boron Doped Diamond Electrodes with Increased Reactivity for Solar-Driven CO₂ Reduction in Room Temperature Ionic Liquids

